Citation for the published version:

Vázquez-Semadeni, E., Zamora-Avilés, M., Galván-Madrid, R., & Forbrich, J. (2018). Molecular Cloud Evolution VI. Measuring cloud ages. Monthly Notices of the Royal Astronomical Society, 479 (3). DOI: 10.1093/mnras/sty1586

Document Version:

Final published version

Link to the final published version available at the publisher:

https://academic.oup.com/mnras/article/479/3/3254/5039668

Molecular cloud evolution – VI. Measuring cloud ages

Enrique Vázquez-Semadeni,[1][*] Manuel Zamora-Avilés,[1,2] Roberto Galván-Madrid[1] and Jan Forbrich[3,4]

[1]*Instituto de Radioastronomía y Astrofísica, UNAM. Apdo. Postal 72-3 (Xangari), Morelia, Michoacán 58089, México*
[2]*Department of Astronomy, University of Michigan, 311 West Hall, 1085 S. University Ann Arbor, MI 48109, USA*
[3]*Centre for Astrophysics Research, School of Physics, Astronomy and Mathematics, University of Hertfordshire, College Lane, Hatfield AL10 9AB, UK*
[4]*Harvard-Smithsonian Center for Astrophysics, 60 Garden Street, Cambridge, MA 02138, USA*

ABSTRACT

In previous contributions, we have presented an analytical model describing the evolution and star formation rate (SFR) of molecular clouds (MCs) undergoing hierarchical gravitational contraction. The cloud's evolution is characterized by an initial increase in its mass, density, SFR, and star formation efficiency (SFE), as it contracts, followed by a decrease of these quantities as newly formed massive stars begin to disrupt the cloud. The main parameter of the model is the maximum mass reached by the cloud during its evolution. Thus, specifying the instantaneous mass and some other variable completely determines the cloud's evolutionary stage. We apply the model to interpret the observed scatter in SFEs of the cloud sample compiled by Lada et al. as an evolutionary effect so that, although clouds such as California and Orion A have similar masses, they are in very different evolutionary stages, causing their very different observed SFRs and SFEs. The model predicts that the California cloud will eventually reach a significantly larger total mass than the Orion A cloud. Next, we apply the model to derive estimated ages of the clouds since the time when approximately 25 per cent of their mass had become molecular. We find ages from ∼1.5 to 27 Myr, with the most inactive clouds being the youngest. Further predictions of the model are that clouds with very low SFEs should have massive atomic envelopes constituting the majority of their gravitational mass, and that low-mass clouds ($M \sim 10^3$–$10^4 M_\odot$) end their lives with a mini-burst of star formation, reaching SFRs ∼300–500$M_\odot$ Myr^{-1}. By this time, they have contracted to become compact (∼1 pc) massive star-forming clumps, in general embedded within larger giant molecular clouds.

Key words: stars: formation – ISM: clouds – ISM: evolution – ISM: kinematics and dynamics – ISM: structure.

1 INTRODUCTION

The lifetime of molecular clouds (MCs) remains an active research topic in the study of the interstellar medium and star formation, and most recent studies, both observational and theoretical, place this lifetime at a few times 10^7 yr for clouds in the 10^5–$10^6 M_\odot$ mass range (e.g. Blitz & Shu 1980; Kawamura et al. 2009; Zamora-Avilés, Vázquez-Semadeni & Colín 2012; Zamora-Avilés & Vázquez-Semadeni 2014; Lee, Miville-Deschênes & Murray 2016). In addition, several observational studies have suggested that the star formation rate (SFR) of the clouds appears to increase over their lifetimes. For example, studies of young clusters embedded in moderate-mass MCs ($\sim 10^4 M_\odot$) (e.g. Palla & Stahler 1999, 2000;

Da Rio et al. 2010) have shown that their age histograms contain a large majority of young (1–2 Myr) objects, but also a tail of older (up to several Myr) ones suggesting an accelerating star formation activity, sometimes followed by a subsequent decline (see also Povich et al. 2016; Schneider et al. 2018). In addition, Kawamura et al. (2009) reported a clear evolutionary process over the lifetime of giant molecular clouds (GMCs; of masses $\sim 10^5$–$10^6 M_\odot$) in the Large Magellanic Cloud, evidenced by the increasing number of massive stars across the sequence of GMC 'classes' proposed by those authors. Finally, on the basis of the large scatter in the observed star formation efficiency (SFE) in Milky Way GMCs, Lee et al. (2016) have concluded that the SFR in those clouds must also be time variable. Numerical simulations of MC formation and evolution also exhibit time varying, increasing SFRs during their early stages (e.g. Vázquez-Semadeni et al. 2007; Hartmann, Ballesteros-Paredes & Heitsch 2012). Also, in the presence of stellar feedback,

at late times the SFRs reach a maximum and begin to decrease again (e.g. Vázquez-Semadeni et al. 2010; Colín, Vázquez-Semadeni & Gómez 2013). Vázquez-Semadeni, González-Samaniego & Colín (2017) have recently shown that the simulations of Colín et al. (2013) in fact produce stellar age histograms highly resemblant of the observed ones (Palla & Stahler 1999, 2000; Da Rio et al. 2010), and reproduce observed radial age gradients in clusters (Getman et al. 2014) as well as bottom-heavy stellar initial mass functions (IMFs) in scattered regions of massive star formation (Povich et al. 2016).

However, most existing models for the SFR in MCs (e.g. Krumholz & McKee 2005; Hennebelle & Chabrier 2011; Padoan & Nordlund 2011; Federrath & Klessen 2012) are based on the assumption that the clouds are near a state of virial equilibrium between turbulence and self-gravity and are therefore in a stationary state. They make predictions for an equally stationary quantity, the SFE per free-fall time ($\epsilon_{\rm ff}$, the fraction of a MC's mass that gets converted into stars per average free-fall time of the cloud) as a function of the parameters of the turbulence. This type of models may be adequate for predicting time- or space-averaged values of the SFR, but cannot describe the evolution of the SFR in individual clouds if these evolve.

A different class of models has been presented by Zamora-Avilés et al. (2012, hereafter Paper I), Zamora-Avilés & Vázquez-Semadeni (2014, hereafter Paper II), Lee et al. (2016), Völschow, Banerjee & Körtgen (2017), and Burkhart (2018), who have specifically included the time dependence of the SFR. In particular, in Papers I and II we presented a model of MC evolution (hereafter, the ZV14 model), in which we assumed that MCs are in general formed by converging flows (*not* collisions of pre-existing clouds) in the warm neutral medium. The collisions produce layers of cold, dense atomic gas through non-linear triggering of the thermal instability (e.g. Ballesteros-Paredes, Hartmann & Vázquez-Semadeni 1999; Hennebelle & Pérault 1999; Koyama & Inutsuka 2000; Walder & Folini 2000; Audit & Hennebelle 2005; Heitsch et al. 2005; Vázquez-Semadeni et al. 2006). These layers start out thin, and grow in thickness (and surface density) at constant volume density (Vázquez-Semadeni et al. 2006) until they become Jeans unstable and begin to contract gravitationally (Vázquez-Semadeni et al. 2007; Heitsch et al. 2008). Thus, in the ZV14 model, we assumed that the clouds begin to undergo gravitational collapse as soon as they reach their thermal Jeans mass, having started from cold atomic gas conditions. However, the collapse is slow during the early stages (e.g. Burkert & Hartmann 2013) and moreover clouds continue to accrete mass from the converging flows. Thus, the clouds generally reach masses significantly larger than their thermal Jeans mass.

The immediate implication of the assumption of cloud contraction in the ZV14 model is that the SFR of the clouds must be increasing over time. Theoretically, this can be understood in the sense that, as the cloud contracts, its mean density increases, and therefore the fraction of mass at high densities (i.e. with short free-fall times) also increases. This high-density tail of the density distribution is the source of the 'instantaneous' SFR of the cloud in the ZV14 and other (Krumholz & McKee 2005; Hennebelle & Chabrier 2011; Padoan & Nordlund 2011; Federrath & Klessen 2012) models. Thus, in the ZV14 model, as the mean density increases, so does the mass fraction undergoing instantaneous collapse, and the SFR increases. Paper I showed that the predicted increase in the SFR was consistent with the observed age histograms in embedded clusters (Palla & Stahler 1999, 2000) and with the evolutionary sequence for GMCs in the LMC proposed by Kawamura et al. (2009), in

both time-scales and stellar content. In Paper II, it was furthermore shown that suitable temporal averages of the ZV14 model reproduce the observed SFRs of nearby MCs, while ensemble averages, with an appropriate weighting by a cloud mass spectrum, reproduce the locations of full galaxies in an SFR versus dense gas mass diagram (Gao & Solomon 2004; Lada et al. 2012).

The ability of the time-dependent ZV14 model to predict the evolution of several cloud properties simultaneously (see Paper II) suggests the possibility of applying it to estimate the ages of MCs. This is possible because the model predicts a one-parameter family of model clouds, where the main parameter is the total system mass[1]; that is, the total mass in the converging streams that eventually undergoes a transition to the cold phase. The evolution of all the other relevant physical quantities of the model clouds, such as instantaneous dense mass, density, size, SFR, and SFE, is self-consistently solved by the model, and so, if any two of those can be measured simultaneously, they can constrain the model to determine its total mass and evolutionary stage.

In the present letter we present such an application to the cloud sample compiled by Lada, Lombardi & Alves (2010, hereafter LLA10). Those authors presented infrared extinction data for a set of 11 nearby, relatively low-mass MCs, which included an estimate of the total cloud mass (mass within the $A_K = 0.1$ extinction contour), the fraction of 'dense' gas mass (mass above the $A_K = 0.8$ contour, which they estimate corresponds to the mass at densities larger than 10^4 cm^{-3}), and an estimate of the instantaneous SFE of each cloud given by the ratio of the number of young stellar objects (YSOs) to the total cloud mass.[2]

The data from LLA10 shows a very large scatter of observed SFEs, with a factor of ∼50 between the largest and the smallest reported SFEs. Those authors note, however, that, similarly to what happens for whole galaxies (Gao & Solomon 2004), the observed SFEs appear to be proportional to the *dense* ($n \gtrsim 10^4$ cm^{-3}) gas mass fraction. Here, we show that this scatter can be understood in terms of the clouds being in different evolutionary stages, and provide estimates for their ages, profiting from the fact that the compilation by LLA10 contains all the necessary information to constrain the ZV14 model to predict the instantaneous SFE and thus infer the clouds' age.

The paper is organized as follows. In Section 2, we give a brief review of the ZV14 model and of the LLA10 data. In Section 3, we present a comparison of the observed SFEs of the clouds with the values predicted by the model at the observed combinations of total cloud masses and the dense gas masses, showing a good match to within factors of a few. In Section 4, we discuss some limitations and implications of our model, as well as how it compares to other models for the SFR in clouds. Finally, in Section 5, we present a summary and draw some conclusions.

---

[1] The model, of course, also depends on the turbulent parameters, but because it assumes that the initial conditions are those of the cold atomic gas, these properties are assumed to be fixed, and so the only free parameter is the total mass of gas accreted by the cloud from the warm diffuse medium.

[2] It is important to note that Evans et al. (2009) also reported SFRs and SFEs for a cloud sample that significantly overlaps with that of LLA10, but the SFRs reported by Evans et al. (2009) are significantly larger than those of LLA10. This is in part due to different extinction cut-off definitions and in part to different conversions from A_V to mass. Since our model considers the mass of all of the cold gas without regard to whether it is atomic or molecular, the lower extinction cut-offs of LLA10 are more representative of the system described by our model.

2 THE MODEL

In this section, we provide a brief qualitative description of the ZV14 model. This model aims at representing the main mechanism of GMC formation, namely the compression of diffuse warm gas from the interarm region as it enters the gravitational potential well of a stellar spiral arm under solar neighbourhood conditions (see e.g. the review by Molinari et al. 2014). We refer the reader to Papers I and II for a detailed discussion of the model equations.

The ZV14 model essentially tracks the evolution of the mass budget in clouds that are born as the result of a non-linearly triggered phase transition from the warm to the cold neutral atomic medium (the WNM and CNM, respectively) by transonic compressions in the WNM, as routinely observed in numerical simulations of dense cloud formation (e.g. Passot, Vazquez-Semadeni & Pouquet 1995; Ballesteros-Paredes et al. 1999; Hennebelle & Pérault 1999; Koyama & Inutsuka 2002; Audit & Hennebelle 2005; Heitsch et al. 2005; Vázquez-Semadeni et al. 2006). In such simulations, the convergence of the flows *non-linearly* triggers a phase transition from the WNM to the CNM. In this type of flows, the size of the forming cloud is not given by the most unstable scale of the thermal instability as in the linear case, but rather, by the transverse scale of the compressive motion acting on the WNM, because it coherently induces the transition over a large area, producing a thin sheet of cold atomic gas (Vázquez-Semadeni et al. 2006). Subsequently, the cold gas sheet often fragments into smaller clumps, but the ensemble of small clumps begins to contract gravitationally as soon as it gathers a mass larger than its thermal Jeans mass (Vázquez-Semadeni et al. 2007).

The large-scale compressions can be driven by either large-scale gravitational effects (e.g. the stellar spiral potential or Parker instabilities) or by generic large-scale turbulent motions in the WNM. The mass flux into the cloud is assumed to last for 25 Myr, and to be given by $\dot{M} = \pi \rho_W \sigma_W R_{cl}^2$, where $\rho_W = 1\,\mathrm{cm}^{-3}$ is the density of the WNM, and corresponds to the mean density of the ISM in the solar neighbourhood, which is at the lower end of the thermally unstable range of the atomic ISM (e.g. Field, Goldsmith & Habing 1969; Wolfire et al. 2003); $\sigma_W = 10\,\mathrm{km\,s}^{-1}$ is the velocity dispersion also in the WNM, and R_{cl} is the radius of the initial flattened, circular cloud. This radius, and the total duration of the mass flow, determine the total mass accreted by the cloud over its lifetime, M_{tot}. However, this quantity is quite elusive, and in fact may never be observed as the cloud's mass, since cloud erosion by feedback may start before all the diffuse gas is converted to dense gas. Therefore, throughout the paper we characterize the model clouds instead by the maximum mass they reach during their evolution, M_{max}, which we use as the single control parameter of the model hereinafter.

The cloud is assumed to have moderately supersonic turbulence (sonic Mach number $M_s \sim 3$), as suggested by the studies of Koyama & Inutsuka (2002), Heitsch et al. (2005), Audit & Hennebelle (2005), and Banerjee et al. (2009), and to start their existence as thin, mostly atomic clouds, similar to those observed by Heiles & Troland (2003). The clouds' mass grows by continuing accretion of warm atomic material at roughly constant volume density (but increasing their thickness and column density), as described in Vázquez-Semadeni et al. (2006), until they become Jeans unstable, and begin to collapse (Vázquez-Semadeni et al. 2007, 2009). The collapse is followed numerically, assuming the cloud has a flattened geometry and a constant thickness, similarly to what is observed in numerical simulations (e.g. Vázquez-Semadeni et al. 2007, 2011; Heitsch & Hartmann 2008; Banerjee et al. 2009; Clark et al. 2012).

The model explicitly assumes that the strongly supersonic motions observed in MCs ($M_s \gtrsim 10$) are dominated by infall, so that the motions corresponding to true turbulence remain at a roughly constant level, dictated by both the accretion (e.g. Hunter et al. 1986; Vishniac 1994; Walder & Folini 2000; Koyama & Inutsuka 2002; Heitsch et al. 2006; Vázquez-Semadeni et al. 2006) and the collapse flows (e.g. Vázquez-Semadeni, Cantó & Lizano 1998; Klessen & Hennebelle 2010; Robertson & Goldreich 2012; Murray & Chang 2015), assuming that the turbulent kinetic energy injected by the accretion or the collapse counteracts turbulent dissipation to maintain a roughly constant, moderate turbulence level. This is consistent with the observation in numerical simulations that the turbulence generated by the accretion or the collapse is never sufficient to halt or significantly delay the collapse (e.g. Vázquez-Semadeni et al. 2007; Heitsch & Hartmann 2008; Banerjee et al. 2009; Ibáñez-Mejía et al. 2016; Murray et al. 2017).

Thus, we assume a lognormal probability density function (PDF) for the density field (Vázquez-Semadeni 1994) having a constant width, corresponding to the assumed Mach number of the initial conditions ($M_s = 3$). We adopt the prescription by Federrath, Klessen & Schmidt (2008), with a compressible-to-solenoidal b parameter corresponding to half the energy in each type of modes. The collapse of the cloud, and the corresponding increase in the cloud's mean density, are modelled by continuously shifting the mean density implied by the PDF to the instantaneous mean density of the cloud.

Similarly to what is done in other models for the SFR (Krumholz & McKee 2005; Hennebelle & Chabrier 2011; Padoan & Nordlund 2011; Federrath & Klessen 2012), the instantaneous SFR is then computed by calculating the mass at densities $n > n_{SF}$ and dividing it by the free-fall time at that density. The density n_{SF} is a free parameter of the model, which was calibrated in Paper I by matching the SFR predicted by the model to that observed in a numerical simulation of a cloud of similar mass. The resulting value of $n_{SF} = 10^6\,\mathrm{cm}^{-3}$ has remained fixed in all subsequent applications of the model.

Once the instantaneous SFR is computed, the model is advanced in time to compute the corresponding increment in the stellar mass, which is subtracted from the dense gas mass. Given the total stellar mass at this time, a standard IMF (Kroupa 2001) is used to compute the instantaneous number of massive ($M > 8M_{\odot}$) stars in the cloud, and then the instantaneous mass ionization rate on the cloud is computed using the prescription from Franco, Shore & Tenorio-Tagle (1994). Over the corresponding time-step, the ionized mass is then also subtracted from the cloud's mass, and the cycle is repeated.

In summary, the model tracks the cloud's mass budget over time, according to the symbolic equation (Paper I)

$$M_{cl}(t) = \int_0^t \dot{M}_{inf}(t')\tilde{\ }\mathrm{d}t' - M_*(t) - M_I(t), \qquad (1)$$

where $M_{cl}(t)$ is the instantaneous cloud (i.e. dense, cold) mass, $\dot{M}_{inf}(t)$ is the mass accretion rate on to the cloud from the WNM inflows,[3] $M_*(t)$ is the instantaneous mass in stars, and $M_I(t)$ is the total mass that has been ionized by stellar feedback. The detailed

---

[3]Strictly speaking, the accretion does not need to be due to warm diffuse gas, and may refer to *any* kind of accretion. However, if the accretion consisted mainly of dense, cold material similar to that of the cloud, then it should also be part of the collapsing cloud, and a more natural way to represent this in the model would be to consider it as part of the dense gas mass, rather than part of the accretion.

expressions and procedures to derive each one of the terms in this equation are given in Paper I.

The model thus follows, as a function of time, and for a given total mass reservoir, the evolution of the instantaneous dense mass, density PDF, radius, mean volume density, SFR, and SFE, computed as $SFE = M_*/(M_{cl} + M_*)$. Note that, in general, $M_{cl} \leqslant M_{max}$, since the instantaneous mass of the cloud starts from zero and grows as it accretes material from the diffuse medium, and then begins to decrease as the stellar feedback within it begins to erode it.

In addition to these physical quantities, the model can predict the instantaneous mass fraction of gas with density larger than some threshold, under the assumption that the density PDF retains its lognormal form, and simply shifts to higher densities as the cloud contracts gravitationally. For reference, we repeat in Fig. 1 the evolution of the dense gas mass and the stellar mass (left-hand panel), the SFR (middle panel) and the SFE (right-hand panel) for clouds of masses 10^3, 10^4, 10^5, and $10^6 M_\odot$ (black, blue, green, and red lines, respectively), as first shown in Paper II. Note that, in these figures, $t = 0$ denotes the time when the WNM streams first collide, and so the cloud has zero mass at $t = 0$.

Note that the assumption that the density PDF remains lognormal is a questionable assumption of our model, since it is now well known that the density PDF instead evolves by developing a power-law tail at high densities (e.g. Kainulainen et al. 2009; Ballesteros-Paredes et al. 2011; Kritsuk, Norman & Wagner 2011; Girichidis et al. 2014; Lombardi, Alves & Lada 2015; Lin et al. 2016). However, it has been suggested by Kritsuk et al. (2011) that the power-law tail of the PDF at high densities is the result of the development of highly peaked power-law radial density profiles, which translate into a power-law density PDF. That is, this tail is the result of the presence of *already collapsing structures*. In our model, the density PDF represents the *turbulent seeds* from which collapse starts, and so in Paper I we argued that the relevant PDF is that of the turbulent fluctuations *before* they begin to collapse, which is known to be lognormal (Vázquez-Semadeni 1994), and is the PDF routinely considered in models for the SFR and the IMF based on the collapse of density fluctuations (Padoan & Nordlund 2002; Krumholz & McKee 2005; Hennebelle & Chabrier 2008, 2011; Padoan & Nordlund 2011; Federrath & Klessen 2012; Hopkins 2012). Once the fluctuations begin to collapse, they are already 'on route' to forming stars, and thus they are already counted by the model as a star that will form after a free-fall time. Thus, their excess density should not be considered as the new initial density of a subsequent collapse. For this reason, we opt for assuming that the density PDF of the seed turbulent fluctuations retains its original lognormal form, and representing the global collapse of the cloud by a shift in the peak of the PDF to higher densities as dictated by the increase in the mean density of the cloud.

Nevertheless, a recent study by Burkhart (2018) has presented a model for the SFR similar to ours, but precisely taking into account the development of a power law in the high-density range of the PDF rather than shifting the entire PDF to higher densities as we do, and obtaining similar results to ours. This suggests that, to first order, the two methods for describing the evolution of the PDF are roughly equivalent.

3 RESULTS

As discussed in Section 2, the ZV14 model predicts the evolution of several physical quantities of a cloud of given total mass as a function of time. Thus, in general, the model requires two parameters (total mass and age) to be specified for a cloud in order to

completely determine its current evolutionary state. However, in general, the age of the cloud is unknown, while several other instantaneous quantities of the cloud, such as its instantaneous mass, dense gas mass fraction, SFE, etc., are observables. Thus, any one of those variables can be used as a proxy for time, in addition to its instantaneous mass. That is, any combination of pairs of observables (e.g. mass-dense mass fraction, mass-mean density, and mass-radius) can constrain the instantaneous evolutionary state of a model cloud.

This capability of the model can then be used to test it against observational data such as those by LLA10. These authors compiled data on total cloud masses (i.e. mass above $A_K = 0.1$), dense gas masses [i.e. mass above $A_K = 0.8$) and SFEs (given in that paper as the instantaneous number of YSOs divided by the clouds' mass) for a sample of 11 nearby clouds. We can thus use one variable – for instance, the dense gas fraction – as the proxy for age, use the mass to constrain the mass parameter of the model, and then compare the observed SFE to that predicted by the model for a cloud of the same instantaneous mass and dense mass fraction. If the model passes this test, then the age it predicts for the cloud can be taken as the actual physical age of the cloud. In what follows we perform this procedure as a test for the model, and then apply it to 'date' the clouds in the LLA10 sample. For convenience, in the second to fourth columns of Table 1 we reproduce the LLA10 data relevant for our study. In the fifth column, we then write the SFE implied by those data, defined as

$$SFE = \frac{M_*}{M_* + M_{cl}} = \frac{0.5 N_{YSO}}{0.5 N_{YSO} + M_{cl}}, \qquad (2)$$

where N_{YSO} is the instantaneous number of YSOs, and $M_* = 0.5 M_\odot N_{YSO}$ is the total stellar mass, assuming that the mean stellar mass is $0.5 M_\odot$. The first equality is also the definition of the SFE in the ZV14 model, since it computes the instantaneous stellar mass during the evolution of a model cloud.

Fig. 2 shows the evolutionary tracks of model clouds of various total masses (indicated by the labels next to each line) in a diagram of instantaneous cloud mass versus instantaneous dense gas mass (i.e. mass at densities $n \geqslant 3 \times 10^4$ cm^{-3}), which we take as a proxy for LLA10's mass above $A_K = 0.8$, and which we use as a proxy for the evolutionary time (or cloud age). Each evolutionary track consists of two coloured lines: one showing the evolution of the SFE for each track, following the continuous colour bar shown at the top left of the figure, and one giving the age of the model cloud since 25 per cent of its mass can be considered molecular (see below), in 2-Myr intervals, following the segmented colour bar shown at the top right. Also shown in this plot are symbols of various shapes corresponding to each of the clouds from the LLA10 sample. Their location corresponds to the reported total and dense gas masses, and their colour corresponds to the reported SFE as given in the fifth column of Table 1. This SFE can thus be compared to the SFE of the nearest model evolutionary track at the location of the point. We have chosen to show models whose evolutionary tracks fall close to the location of the LLA10 data points.

It is clearly seen from Fig. 2 that the colour of the points (the observed SFEs of the clouds in the sample) and those of the model clouds at the locations of the points are similar, implying that the observed SFEs of the clouds are consistent with their instantaneous total and dense gas masses, as prescribed by our model.

To better quantify the degree of agreement between the predicted and observed SFEs for the LLA10 clouds, in Fig. 3 we plot the value of the SFE predicted by a model cloud that has the same instantaneous cloud mass and dense gas fraction pair, (M_{cl}, f_d),
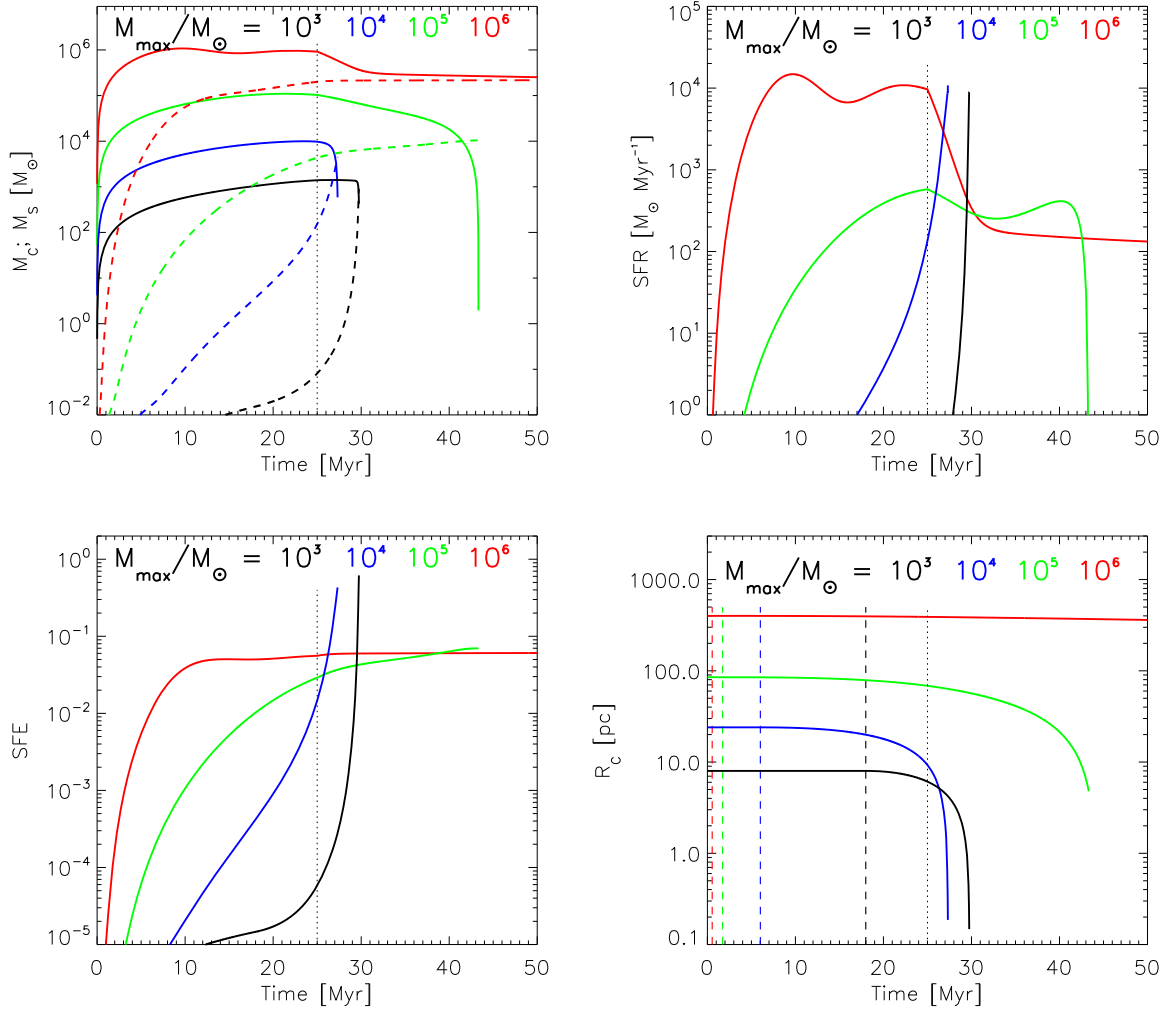
Figure 1. Time evolution of the cloud mass and mass in stars (top left-hand panel, solid and dashed lines, respectively), SFR (top right-hand panel), SFE (bottom left-hand panel), and radius (bottom right-hand panel) for clouds with $M_{max} = 10^3$, 10^4, 10^5, and 10^6 M$_\odot$ (black, blue, green, and red lines, respectively). The vertical dotted black line is the time at which the accretion stops ($t = 25$ Myr). (Plots reproduced from Paper II).

Table 1. Observed parameters of the cloud sample of LLA10.

Cloud name	Total mass[a] (M$_\odot$)	Dense mass[b] (M$_\odot$)	Number of YSOs	Observed SFE[c] (per cent)
Orion A	67 714	13 721	2862	2.1
Orion B	71 828	7261	635	0.44
California	99 930	3199	279	0.14
Perseus	18 438	1880	598	1.6
Taurus	14 964	1766	335	1.1
Ophiuchus	14 165	1296	316	1.1
RCrA	1137	258	100	4.2
Pipe	7937	178	21	0.13
Lupus 3	2157	163	69	1.6
Lupus 4	1379	124	12	0.43
Lupus 1	787	75	13	0.82

Notes. [a]Mass within the $A_K = 0.1$ contour.
[b]Mass within the $A_K = 0.8$ contour.
[c]According to equation (2).

versus the observed value. The dotted line shows the identity line. Although with significant scatter, a clear correlation is seen to exist between the model-predicted and the observed values of the SFE. Thus, we propose that the observed scatter in the SFEs of the LLA10 clouds can be interpreted simply as a consequence that the clouds are observed at different evolutionary stages.

For reference, in Table 2 we list (a) the maximum mass, M_{max}, of the model cloud with the same instantaneous mass and instanta-
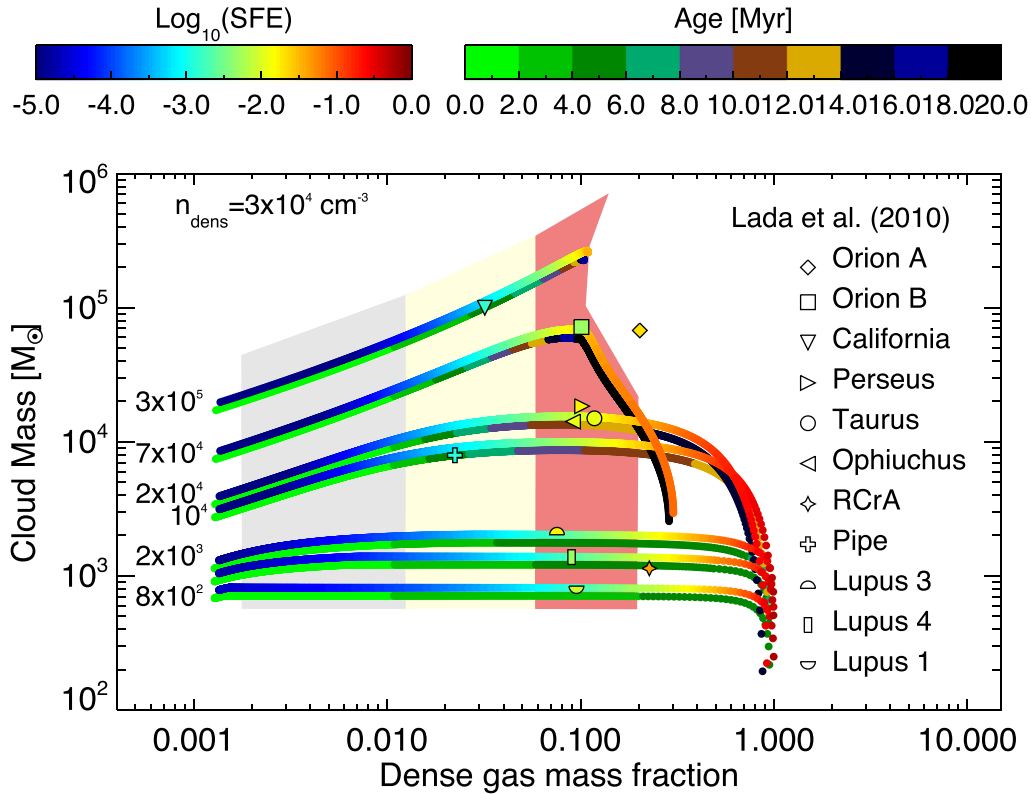
Figure 2. Instantaneous cloud mass versus instantaneous dense gas mass fraction (i.e. mass at densities $n \geqslant 3 \times 10^4 \, \text{cm}^{-3}$) of model clouds of various total masses (indicated by the labels next to each line). The tracks consist of two coloured lines. The lines using the colour bar at the top left indicate the instantaneous SFE of the model. The lines using the colour bar at the top right show the cloud age since becoming 25 per cent molecular, in 2-Myr intervals. The points show the clouds from the LLA10 compilation, and their colours indicate the reported SFE, using equation (2). The gray-, cream-, and rose-coloured vertical bands, respectively, indicate the evolutionary periods during which 25, 50, and 75 per cent of the gas mass is between $10^3 \, \text{cm}^{-3}$ (left edge of each band) and $3 \times 10^3 \, \text{cm}^{-3}$ (right edge of the band).
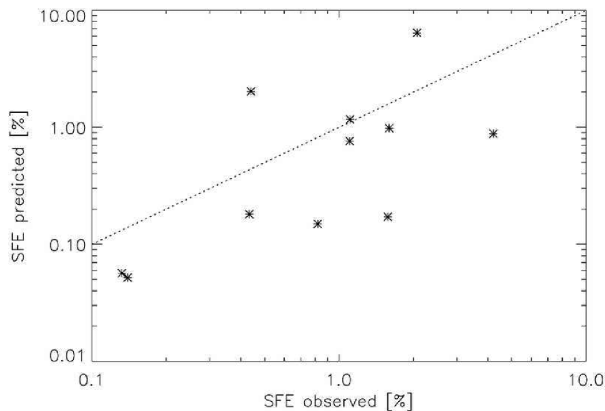

Figure 3. Value of the SFE predicted by a model cloud that has the same instantaneous cloud mass and dense gas fraction pair, $(M_{\text{cl}}, f_{\text{d}})$, as each one of the clouds in the LLA10 compilation, plotted against the corresponding observed value.

neous dense fraction; (b) the SFE of this model cloud at the time when it has these values of the pair $(M_{\text{cl}}, f_{\text{d}})$; and (c) the predicted total age of this model; that is, the time since the moment when the colliding streams first encountered each other.

However, the time at which the WNM streams first encountered each other is of little practical interest, since this event is unobservable. A more interesting age is that since the cloud is already

sufficiently molecular to be identified as an MC. Although our model does not include any chemistry, a first approximation to the molecular fraction can be obtained by measuring the mass fraction above a density high enough that the gas is most likely molecular there. We choose this 'molecular' density as $n_{\text{mol}} = 3 \times 10^3 \, \text{cm}^{-3}$. This value follows from the standard prescription that the time-scale for H_2 molecule formation is $\tau_{H2} \sim 10^9/n$ yr (McCrea & McNally 1960). Thus, at the density n_{mol}, the time-scale is $\tau_{H2} \sim 3 \times 10^5$ yr, which is much shorter than the time-scales for MC evolution discussed here. Table 2 thus shows, in the fifth column, the clouds' ages since they became significantly 'molecular'; i.e. since 25 per cent of their mass was at density n_{mol} or larger. We see that the clouds' ages according to this criterion range from $\sim$1.6 to $\sim$27 Myr. Most importantly, there is a general trend that the larger the molecular age, the more efficiently the cloud is forming stars, as prescribed by the ZV14 model. It is worth noting that the 'molecular ages' of the lowest-mass clouds are in general lower than 3 Myr, which may seem contradictory with the fact that some of those clouds (e.g. Lupus and Corona Australis) are known to have evolved class II YSOs (Ansdell et al. 2016; Currie & Sicilia-Aguilar 2011, respectively), which may suggest an age larger than the one we measured. The correct way to interpret this is that those objects formed when the mass of the clouds was dominated by an atomic component, most likely in the form of an atomic envelope, with still less than 25 per cent of the total cloud mass in molecular form.

Finally, in Fig. 2 we also show three coloured vertical bands that aim to provide a proxy for the evolution of the molecular fraction

Table 2. Modelled parameters for the cloud sample of LLA10.

Cloud	M_{max} model (M$_\odot$)	Predicted SFE (%)	Time[a] (Myr)	Molecular age[b] (Myr)
Orion A	6.87×10^4	6.4	34.6	27.1
Orion B	6.87×10^4	2.0	24.3	16.8
California	2.65×10^5	0.052	5.47	2.2
Perseus	1.76×10^4	0.98	24.2	10.4
Taurus	1.55×10^4	1.2	24.6	10.1
Ophiuchus	1.55×10^4	0.76	23.8	9.3
RCrA	1.39×10^3	0.88	29.2	2.7
Pipe	9.96×10^3	0.057	18.8	2.3
Lupus 3	2.03×10^3	0.17	27.6	2.5
Lupus 4	1.39×10^3	0.18	28.6	2.1
Lupus 1	8.16×10^2	0.15	33.4	1.6

Notes. [a]Total time since when the WNM streams first collide.
[b]Time since 25% of the cloud's mass exceeded a density of 3×10^3 cm^{-3}.

(f_{mol}) of the gas, assuming that the gas becomes molecular roughly when the volume density is between 1 and 3×10^3 cm^{-3}. Since the cloud is contracting gravitationally, it is becoming denser on average, and thus the fraction of the cloud's mass that is above a certain density threshold increases over time. The gray band covers the interval between the time when 25 per cent of the gas mass is above $n = 10^3$ cm^{-3} (left edge of the bar) and when 25 per cent is above $n = 3 \times 10^3$ cm^{-3} (right edge). The cream- and rose-coloured bands show the corresponding evolutionary intervals for 50 and 75 per cent of the gas mass above these density thresholds.

4 DISCUSSION

4.1 Implications and insights

Our results strongly suggest that the ZV14 model correctly describes, at least to first order, the evolution of MCs and their SF activity, as a consequence of their being in a state of global and hierarchical collapse. The good average match between the observed SFEs and the values predicted by our model for clouds of the same instantaneous mass and dense mass fraction shows that the evolutionary state of a cloud can be determined, at least to first order, when *a pair* of cloud properties are known. This is because the evolutionary model constitutes a one-parameter family of models, where the control parameter is the total mass involved in the accretion and collapse process that forms the cloud. Fortunately, although this total mass is in general unknown, it suffices to know the *instantaneous* cloud mass, since, once it is combined with another parameter, such as the dense fraction as we have done here, it uniquely determines the both the total mass and the evolutionary stage of the model. The model then allows to specify an age for the cloud.

A number of points are worth noting. First, we remark that the converging-flow set-up is not essential for the evolution of the SFR in our model. What determines this evolution is the process of collapse. The converging flows are mostly important for *forming* a cloud when there was none before. This is important to understand why a cloud *begins* to collapse at some point. Otherwise, this point in time (the onset of collapse) would be unconstrained. In the model, this happens after the cloud reaches its thermal Jeans mass, due to the accretion. But, since this accretion rate is assumed to remain constant, it becomes progressively less important compared to the increase in the cloud's mean density induced by the collapse as the cloud evolves. This is especially true for the lower-mass clouds,

which have small cross-sections for accreting diffuse gas. So, the accretion becomes a secondary ingredient at late stages, and the evolution proceeds towards increasing domination by the collapse.

Secondly, our result that the predicted and observed SFEs correlate well for clouds of a given instantaneous mass and dense gas fraction could be interpreted as to simply mean that the number of stars will be proportional to the dense gas mass if the dynamical time for collapse in that gas is constant.[4] However, it is important to note that our model contains no intrinsic assumption about any proportionality between the dense gas mass and the number of stars, or the SFR. Rather, in the model, the dense gas mass and the SFR are, respectively, given by the mass fraction above the density threshold for defining 'dense gas', $n_d = 3 \times 10^4$ cm^{-3}, and the mass fraction above the critical density for star formation, $n_{SF} = 10^6$ cm^{-3}. Both of these quantities depend on the instantaneous values of the mean and standard deviation (assumed constant) of the density PDF. The ratio between these two mass fractions is not constant over time, because the density PDF is not linear with density, and thus, as it shifts to higher densities over time, the ratio of these two masses varies. Moreover, the instantaneous SFE is given by the total stellar mass (which is proportional to the time integral of the SFR) divided by the instantaneous cloud mass. The latter, in turn, depends on the accretion, star formation, and mass-loss rates. Thus, the resulting match between the observed and predicted SFEs constitutes a true test of the model, and not just the result of an imposed proportionality between the dense gas mass and the number of stars. Rather, this proportionality is then a prediction of the model.

Thirdly, note that model clouds with different values of the maximum mass may have the same value of their instantaneous cloud mass, but at different evolutionary stages. For example, although the instantaneous masses of the Orion A, Orion B, and California clouds are similar, the fact that the California cloud has a much lower SFE than the Orion A cloud implies, according to the model, that the California cloud system involves a larger total mass, but is at an earlier evolutionary stage. Indeed, as seen in Table 2, the model cloud that fits both Orion clouds reaches a maximum cold-gas (cloud) mass of $\sim 6.9 \times 10^4$ M$_\odot$, while the model cloud fitting the California cloud reaches a maximum mass of $\sim 2.65 \times 10^5$ M$_\odot$. This shows that the evolution of MCs inherently relates the accretion on to the cloud and its SF activity, since the mass growth of the clouds occurs simultaneously with the increase in their SFR.

---

[4]We thank the referee for noting this.

It is also important to remark that the model implies that the transition of the cloud from being atomic-dominated to molecule-dominated occurs gradually and simultaneously with the increase in its star-forming activity. For example, it can be seen from Fig. 2 that low-SFE clouds such as the California and the Pipe clouds are expected to be only roughly 50 per cent molecular (they lie in the middle of the yellow band), implying that they should have about 50 per cent of their gravitational mass still in atomic form. This possibility is usually overlooked when the gravitational binding of the clouds is estimated via the clouds' molecular mass.

4.2 The final mini-burst stages

Finally, it is worth remarking that the model predicts quite large SFRs and SFEs at the final stages of low-mass clouds. For example, it is seen from the top right and bottom left panels of Fig. 1 that the model clouds with $M_{max} = 10^3 M_\odot$ and $10^4 M_\odot$ (respectively, the black and blue curves) reach peak SFRs $\sim 10^4 M_\odot$ Myr^{-1}, and final SFEs ~ 40 per cent and 60 per cent, respectively. These are in general not associated with low-mass clouds. However, it should be kept in mind that the model follows the evolution of the gas mass throughout its evolution, from the cold atomic cloud stage (Vázquez-Semadeni et al. 2006) to the HII region stage. The large final SFRs and SFEs correspond to stages when a few OB stars and developed HII regions must be present.

This can be exemplified by comparing the model prediction with a strongly active region, such as the OMC-1 clump and its associated Orion Nebula and the Orion Nebula Cluster (ONC). According to the data collected in Vázquez-Semadeni et al. (2009), the OMC-1/ONC system has a size ~ 1.2–1.5pc, contains a cold gas mass $M_{gas} \approx 2200 M_\odot$ (Bally et al. 1987) and ~ 1600 stars (Tobin et al. 2009), implying a stellar mass of 500–800$M_\odot$, assuming a mean stellar mass $M_* = 0.3$–0.5$M_\odot$. Moreover, its estimated age is $\lesssim 2$ Myr (Hillenbrand 1997). Therefore, this system has had an average SFR of 250–400$M_\odot$ Myr^{-1} over the last 2 Myr, and has a present observed SFE ~ 25–33 per cent. A recent estimate for the SFE of the OMC-1/ONC system by Da Rio, Tan & Jaehnig (2014) based on estimates of the free-fall time implied by the mass distribution yields an SFE ~ 30–50 per cent.

This can be compared to the evolution of the $10^4 M_\odot$ model cloud shown in Fig. 1. From the top-left panel of this figure, it can be seen that at $t \approx 26.8$ Myr, $M_* \approx 10^3 M_\odot \sim 1/3 M_{gas}$, for an SFE= $M_*/(M_{gas} + M_*) \approx 25$ per cent. Moreover, from the bottom right-hand panel of Fig. 1, we see that the cloud's radius is decreasing very rapidly, and has a size of a few parsecs.

To compute the average SFR of this model cloud, $\langle SFR \rangle$, over the last 2 Myr, we note from the top-right panel of Fig. 1 that, over the time interval $24.8 \leqslant t < 26.8$ Myr, the SFR may be approximated by an exponential function of time. To estimate the characteristic time-scale of this function, we note that at $t \approx 26.8$, the SFR of the $10^4 M_\odot$ model is SFR($t = 26.8$) $\sim 3 \times 10^3 M_\odot$ Myr^{-1}, while 2 Myr earlier, SFR($t = 24.8$) $\sim 100 M_\odot$ Myr^{-1}. Fitting a straight line in log-lin SFR-t space, we find

$$SFR(t) \approx SFR(t_0) \exp\left(\frac{t - t_0}{\tau}\right),$$

where $\tau \approx 0.59$ Myr. Averaging this function over the time interval $24.8 \leqslant t < 26.8$ Myr, we obtain $\langle SFR \rangle \approx 880 M_\odot$ Myr^{-1}.

This estimate is two to three times larger than the observed $\langle SFR \rangle$ of the OMC1/ONC system. However, due to the steepness of the SFR(t) curve, this estimate is highly sensitive to the choice of time interval. For example, if the starting point of the averaging interval is

taken as $t = 24$ Myr instead of 24.8, the resulting $\langle SFR \rangle$ is $\sim 470 M_\odot$ Myr^{-1}, suggesting that, within the uncertainties, the evolution of the SFR described by our model is roughly consistent with observations. Moreover, we note that the SFE, which is the result of the integrated SF activity over the evolution of the cloud, is fully consistent with that observed for the OMC-1/ONC system. Thus, we conclude that the final SF burst of the low-mass regions predicted by our model adequately describes the evolution of these systems.

4.3 Assumptions and limitations

Our model is of course subject to a number of assumptions that limit its predictive ability to only order-of-magnitude precision. Besides the assumption of a persistent lognormal PDF discussed in Section 2, which may or may not be a problem, another limitation of our model is that it only considers collapse and cloud destruction by photoionizing radiation. It neglects possible delay of the collapse by magnetically supercritical magnetic fields, additional cloud destruction/dispersal processes such as supernovae, stellar winds, etc., and, particularly importantly, variations in the accretion rate due to processes other than the inertial mass flux we have considered. All of these mechanisms may be responsible for the significant scatter observed in the plot of predicted-versus-observed SFE (Fig. 3). Another source of uncertainty is that we have used a volume density threshold (3×10^4 cm^{-3}) for comparison to a column density one (LLA10's $A_K = 0.8$ definition of high column density gas), and the correspondence between the two types of density is far from perfect. Nevertheless, using high-volume density gas is actually closer to the physical motivation behind the consideration of high-column density gas, since LLA10 themselves assume that the $A_K > 0.8$ gas is representative of gas with $n > 10^4$ cm^{-3}, on the basis of the assumption that it is the dense gas that is actually responsible for star formation.

Another limitation of our model, in its application for the present study,[5] is that we have assumed that all clouds start from the same initial conditions, namely those of the CNM in the solar neighbourhood, and with the same accretion rate from the WNM. Fluctuations in these initial conditions, in particular in the mean density and temperature of the forming clouds, will cause fluctuations in the clouds' thermal Jeans mass, and therefore in the time of the onset of collapse. This effect surely contributes to the scatter we observe in the predicted-versus-observed SFE plot of Fig. 3.

Finally, yet another idealization of our model is the assumption that the accretion on to the clouds consists exclusively of warm diffuse gas. This is a reasonable first-order approximation for solar neighbourhood conditions, as it is known that, at the solar galacto-centric radius, the azimuthally averaged molecular mass fraction is only 10–20 per cent, and the gas cycles from predominantly atomic to molecular as it passes through the spiral arms (e.g. Koda, Scoville & Heyer 2016). Moreover, since the mean density of the atomic gas at the solar radius is $n_H \sim 1$ cm^{-3} (e.g. Ferrière 2001), this gas is predominantly in the warm phase. Thus, the gas from which the GMCs in the solar neighbourhood form is expected to be WNM.

Nevertheless, in reality, even if the accretion on to the GMCs consists of predominantly-diffuse gas from the interarm region as it enters a spiral arm, it is likely to contain a 'mist' of dense,

---

[5]The initial physical conditions of the model may be specified at will, and, in fact, applications to different environments can be achieved by specifying the appropriate initial conditions for each environment, such as the Central Molecular Zone of the Milky Way, for example.

cold cloudlets. This is because the dense gas seems to not be fully destroyed by stellar feedback, as it exits the previous spiral arm. Instead, only part of it is truly destroyed, while the rest is dispersed into smaller units (Koda et al. 2016). Thus, a more realistic description of the assembly of GMCs would include this mist of cold clumps.

The problem of GMC assembly by diffuse-gas streams containing scattered cold clumps has been investigated numerically by Carroll-Nellenback, Frank & Heitsch (2014). These authors compared two converging-flow simulations, in both of which the mean density of the inflows is $\langle n \rangle = 1 \, \mathrm{cm}^{-3}$, but being uniform in one case, and clumpy in the other. In the latter, there is a substrate of density $n = 0.25 \, \mathrm{cm}^{-3}$ and a mist of clumps of radius 0.55 pc and density $n_c = 15.2 \, \mathrm{cm}^{-3}$. They found that, in the clumpy run, the forming cloud fragments less, collapses later, and acquires more mass, because the substrate's density is lower, implying higher temperatures in the compressed layer, and thus a larger Jeans mass. The clump–clump collisions are not very efficient because their collisional cross-section is small. Thus, once the cloud becomes gravitationally unstable, the global collapse is more focused, and the SFR reaches higher values than in the smooth run, leading to higher final total stellar mass, by a factor of ∼2. Thus, although the presence of dense cloudlets does introduce minor quantitative differences, it does not significantly affect the overall qualitative evolution of the cloud.

5 CONCLUSIONS

In this paper, we have shown that the our ZV14 evolutionary model of collapsing clouds and their SFR captures to order-of-magnitude precision the observed scatter in the SFE of MCs, and provides an interpretation of it in terms of different clouds being at different evolutionary stages, since the model predicts that the SFR of the clouds varies in time, first increasing as the clouds' density increases during collapse, and then decreases as stellar feedback begins to disrupt the clouds. This interpretation is consistent with previous works proposing that an 'uncertainty principle' applies to observations of the SFR in external galaxies below a certain spatial scale, because the observed regions are small enough that local evolutionary differences cannot averaged out over the region, and different regions are caught in different evolutionary states, so that they will display different SFRs at a given gas mass (Kruijssen & Longmore 2014; Kruijssen et al. 2018).

The fact that our model correctly captures the average evolutionary trend of the SFE with other cloud parameters suggests that the dominant mechanisms controlling MC evolution are indeed their global gravitational collapse and their subsequent destruction by stellar feedback, as described by our model, with other processes providing second-order corrections. These are better followed by detailed numerical simulations. However, the model allows an understanding of the fundamental physical underlying processes.

Also, our results imply that the reason higher-density gas appears to correlate linearly with the SFR, while lower-density gas exhibits a looser correlation (e.g. Gao & Solomon 2004; Bigiel et al. 2008; Lada et al. 2012) is not because only the dense gas forms stars, but because it is *closer* in time and space to forming stars than the lower density gas, as suggested by Burkert & Hartmann (2013). In turn, this occurs because of the global collapse of MCs we have proposed (Vázquez-Semadeni et al. 2009), since gravitational collapse is, in general, extremely non-homologous, amplifying density gradients and causing an accelerating gas flow from the low- to the high-density regions.

We stress that, in our model, the clouds do not have a well-defined time at which they are 'born', since their molecular (i.e. dense gas) fraction increases over time. This in turn implies that, especially during the early evolutionary stages of the clouds, the dynamic role provided by the weight of its atomic envelope is important, and cannot be neglected when considering the gravitational boundedness of a cloud.

Finally, our model predicts that low-mass clouds ($M \sim 10^3$–$10^4 \, \mathrm{M}_\odot$) undergo a strong mini-burst of SF at the end of their lives, when they constitute a compact, massive *clump*, generally embedded within a larger, more massive cloud. Although this prediction may appear as counterintuitive at first, because low-mass clouds are in general associated with low SFRs, it must be understood in terms of an *evolutionary* sequence. Although at its initial stages the cloud has sizes ∼10 pc, densities of a few times $100 \, \mathrm{cm}^{-3}$, and SFRs $\sim 10 \, \mathrm{M}_\odot \, \mathrm{Myr}^{-1}$, and therefore corresponds to our standard definition of a 'low-mass cloud', by the time such a gas parcel reaches its final stages, it has contracted to sub-parsec scales and reached densities $n \gtrsim 5 \times 10^3 \, \mathrm{cm}^{-3}$ (see Fig. 1 of Paper II), with SFRs $\gtrsim 300 \, \mathrm{M}_\odot \, \mathrm{Myr}^{-1}$, thus corresponding to our notion of a 'massive clump'. Moreover, since accretion on to the cloud is expected to continue from its environment, this clump is now expected to be part of a larger-mass system, which would correspond to a larger-mass cloud in our model. Thus, the model proposes a unification of the various classes of objects into a general evolutionary picture in which all of the cloud properties such as its mass, density, size, and star formation activity change in time, transiting from quiescent to bursting stages, and then being destroyed by the stellar feedback. Further testing and predictions of the model will be presented in future contributions.

REFERENCES

Ansdell M. et al., 2016, ApJ, 828, 46
Audit E., Hennebelle P., 2005, A& A, 433, 1
Ballesteros-Paredes J., Hartmann L., Vázquez-Semadeni E., 1999, ApJ, 527, 285
Ballesteros-Paredes J., Vázquez-Semadeni E., Gazol A., Hartmann L. W., Heitsch F., Colín P., 2011, MNRAS, 416, 1436
Bally J., Stark A. A., Wilson R. W., Langer W. D., 1987, ApJ, 312, L45
Banerjee R., Vázquez-Semadeni E., Hennebelle P., Klessen R. S., 2009, MNRAS, 398, 1082
Bigiel F., Leroy A., Walter F., Brinks E., de Blok W. J. G., Madore B., Thornley M. D., 2008, AJ, 136, 2846
Blitz L., Shu F. H., 1980, ApJ, 238, 148
Burkert A., Hartmann L., 2013, ApJ, 773, 48
Burkhart B., 2018, ApJ, preprint (arXiv:1801.05428)
Carroll-Nellenback J. J., Frank A., Heitsch F., 2014, ApJ, 790, 37
Clark P. C., Glover S. C. O., Klessen R. S., Bonnell I. A., 2012, MNRAS, 424, 2599
Colín P., Vázquez-Semadeni E., Gómez G. C., 2013, MNRAS, 435, 1701
Currie T., Sicilia-Aguilar A., 2011, ApJ, 732, 24
Da Rio N., Robberto M., Soderblom D. R., Panagia N., Hillenbrand L. A., Palla F., Stassun K. G., 2010, ApJ, 722, 1092

Da Rio N., Tan J. C., Jaehnig K., 2014, ApJ, 795, 55
Evans N. J., II, et al., 2009, ApJS, 181, 321
Federrath C., Klessen R. S., 2012, ApJ, 761, 156
Federrath C., Klessen R. S., Schmidt W., 2008, ApJ, 688, L79
Ferrière K. M., 2001, Rev. Mod. Phys., 73, 1031
Field G. B., Goldsmith D. W., Habing H. J., 1969, ApJ, 155, L149
Franco J., Shore S. N., Tenorio-Tagle G., 1994, ApJ, 436, 795
Gao Y., Solomon P. M., 2004, ApJ, 606, 271
Getman K. V. et al., 2014, ApJ, 787, 108
Girichidis P., Konstandin L., Whitworth A. P., Klessen R. S., 2014, ApJ, 781, 91
Hartmann L., Ballesteros-Paredes J., Heitsch F., 2012, MNRAS, 420, 1457
Heiles C., Troland T. H., 2003, ApJ, 586, 1067
Heitsch F., Hartmann L., 2008, ApJ, 689, 290
Heitsch F., Burkert A., Hartmann L. W., Slyz A. D., Devriendt J. E. G., 2005, ApJ, 633, L113
Heitsch F., Slyz A. D., Devriendt J. E. G., Hartmann L. W., Burkert A., 2006, ApJ, 648, 1052
Heitsch F., Hartmann L. W., Slyz A. D., Devriendt J. E. G., Burkert A., 2008, ApJ, 674, 316
Hennebelle P., Chabrier G., 2008, ApJ, 684, 395
Hennebelle P., Chabrier G., 2011, ApJ, 743, L29
Hennebelle P., Pérault M., 1999, A& A, 351, 309
Hillenbrand L. A., 1997, AJ, 113, 1733
Hopkins P. F., 2012, MNRAS, 423, 2037
Hunter J. H., Jr, Sandford M. T., II, Whitaker R. W., Klein R. I., 1986, ApJ, 305, 309
Ibáñez-Mejía J. C., Mac Low M.-M., Klessen R. S., Baczynski C., 2016, ApJ, 824, 41
Kainulainen J., Beuther H., Henning T., Plume R., 2009, A& A, 508, L35
Kawamura A. et al., 2009, ApJS, 184, 1
Klessen R. S., Hennebelle P., 2010, A& A, 520, A17
Koda J., Scoville N., Heyer M., 2016, ApJ, 823, 76
Koyama H., Inutsuka S. I., 2000, ApJ, 532, 980
Koyama H., Inutsuka S.-I., 2002, ApJ, 564, L97
Kritsuk A. G., Norman M. L., Wagner R., 2011, ApJ, 727, L20
Kroupa P., 2001, MNRAS, 322, 231
Kruijssen J. M. D., Longmore S. N., 2014, MNRAS, 439, 3239
Kruijssen J. M. D., Schruba A., Hygate A. P. S., Hu C.-Y., Haydon D., Longmore S. N., 2018, MNRAS, in press
Krumholz M. R., McKee C. F., 2005, ApJ, 630, 250
Lada J. L., Lombardi M., Alves J. F., 2010, ApJ, 724, 687 (LLA10)
Lada C. J., Forbrich J., Lombardi M., Alves J. F., 2012, ApJ, 745, 190
Lee E. J., Miville-Deschênes M.-A., Murray N. W., 2016, ApJ, 833, 229
Lin Y. et al., 2016, ApJ, 828, 32

Lombardi M., Alves J., Lada C. J., 2015, A& A, 576, L1
McCrea W. H., McNally D., 1960, MNRAS, 121, 238
Molinari S. et al., 2014, in Beuther H., Klessen R. S., Dullemond C. P., Henning T., eds, Protostars and Planets VI. Univ. Arizona Press, Tucson, AZ, p. 125
Murray N., Chang P., 2015, ApJ, 804, 44
Murray D. W., Chang P., Murray N. W., Pittman J., 2017, MNRAS, 465, 1316
Padoan P., Nordlund A., 2011, ApJ, 730, 40
Padoan P., Nordlund, Å., 2002, ApJ, 576, 870
Palla F., Stahler S. W., 1999, ApJ, 525, 772
Palla F., Stahler S. W., 2000, ApJ, 540, 255
Passot T., Vazquez-Semadeni E., Pouquet A., 1995, ApJ, 455, 536
Povich M. S., Townsley L. K., Robitaille T. P., Broos P. S., Orbin W. T., King R. R., Naylor T., Whitney B. A., 2016, ApJ, 825, 125
Robertson B., Goldreich P., 2012, ApJL, 750, L31
Schneider F. R. N. et al., 2018, Science, 359, 69
Tobin J. J., Hartmann L., Furesz G., Mateo M., Megeath S. T., 2009, ApJ, 697, 1103
Vázquez-Semadeni E., 1994, ApJ, 423, 681
Vázquez-Semadeni E., Cantó J., Lizano S., 1998, ApJ, 492, 596
Vázquez-Semadeni E., Ryu D., Passot T., González R. F., Gazol A., 2006, ApJ, 643, 245
Vázquez-Semadeni E., Gómez G. C., Jappsen A. K., Ballesteros-Paredes J., González R. F., Klessen R. S., 2007, ApJ, 657, 870
Vázquez-Semadeni E., Gómez G. C., Jappsen A.-K., Ballesteros-Paredes J., Klessen R. S., 2009, ApJ, 707, 1023
Vázquez-Semadeni E., Colín P., Gómez G. C., Ballesteros-Paredes J., Watson A. W., 2010, ApJ, 715, 1302
Vázquez-Semadeni E., Banerjee R., Gómez G. C., Hennebelle P., Duffin D., Klessen R. S., 2011, MNRAS, 414, 2511
Vázquez-Semadeni E., González-Samaniego A., Colín P., 2017, MNRAS, 467, 1313
Vishniac E. T., 1994, ApJ, 428, 186
Völschow M., Banerjee R., Körtgen B., 2017, A&A, 605, A97
Walder R., Folini D., 2000, Ap&SS, 274, 343
Wolfire M. G., McKee C. F., Hollenbach D., Tielens A. G. G. M., 2003, ApJ, 587, 278
Zamora-Avilés M., Vázquez-Semadeni E., 2014, ApJ, 793, 84 (Paper II)
Zamora-Avilés M., Vázquez-Semadeni E., Colín P., 2012, ApJ, 751, 77 (Paper I)

This paper has been typeset from a TEX/LATEX file prepared by the author.